International Journal of Modern Physics B
Vol. 17, Nos. 22, 23 & 24 (2003) 4123–4138

World Scientific
www.worldscientific.com

EFFECT OF SPONTANEOUS EMISSION NOISE AND MODULATION ON SEMICONDUCTOR LASERS NEAR THRESHOLD WITH OPTICAL FEEDBACK

WING-SHUN LAM*,†, PARVEZ N. GUZDAR† and RAJARSHI ROY*,†,‡

*Department of Physics, University of Maryland, College Park, Maryland, 20742, USA
†IREAP, University of Maryland, College Park, Maryland 20742, USA
‡IPST, University of Maryland, College Park, Maryland 20742, USA

Received 8 August 2002

The dynamical behavior of power dropouts in a semiconductor laser with optical feedback, pumped near threshold current, is strongly influenced by quantum noise. This is clearly demonstrated by experiments with modulations on the pumping current or the feedback strength. For the cases without modulation and with only current modulation, the dropouts occur randomly. However the feedback strength modulation locks the dropout events periodically. By numerically modeling these three cases using the Lang–Kobayashi equations with a stochastic term to take into account spontaneous emission noise, it is shown that the observed behavior of the dropouts can be readily reproduced for all three cases. Noise plays a signifcant role in explaining the observed dropout events. A simple explanation of the observed dropout phenomenon is presented, based on the adiabatic motion of the ellipse formed by the steady state solutions of the rate equations due to slow time modulations of the injection current or the feedback strength.

PACS numbers: 05.40.Ca, 05.45.-a, 42.55.Px, 42.65.-k

1. Introduction

Deterministic chaos occurs in many systems which have irregular and complicated behaviors. However, whether the complexity of a system is due to deterministic chaos, a stochastic source, or a combination of both is sometimes not easy to distinguish. Among these systems, the power dropout phenomenon in semiconductor lasers with optical feedback is a typical example for which the source of the observed chaotic intensity time series has been discussed extensively.[1−13] When a solitary laser pumped very near threshold is subject to reflective feedback from a distant mirror, the output intensity drops to almost zero (dropout), recovers to a steady state output level gradually, and repeats this behavior at irregular intervals.

After decades of study, there are mainly two pictures of the phenomenon. The first one is a stochastic model suggested by Henry and Kazarinov[2] recognizing the importance of quantum noise due to spontaneous emission in initiating the dropouts. They considered small fluctuations in intensity and phase about steady

state values as a result of spontaneous emission and reduced the infinite-dimensional delay differential rate equations (Lang–Kobayashi equations) to an approximate one-dimensional equation of motion in a potential well for the carrier number. A first-passage time problem was thus formulated and the dependence of the mean time interval between dropouts on the feedback strength was estimated. This was later experimentally verified for the operation of the laser near threshold.[6,11] In their study, Henry and Kazarinov did not integrate the stochastic delay differential equations explicitly.

The second picture is of a deterministic nature and was carefully investigated by Sano.[4] Instead of just using a linear analysis, he integrated the delay differential Lang–Kobayashi equations explicitly without noise. In the phase space spanned by the population inversion and the external cavity round trip phase shift, the stable external cavity modes and unstable "antimodes" form an ellipse. As the injection parameter is increased, the stable external cavity modes become unstable via a Hopf bifurcation and then become chaotic through the quasi-periodic route. In the absence of a noise source in the calculation, he explained the dropout phenomenon as a collision between a chaotic attractor and the unstable "antimodes". This explanation provides a detailed insight of the dropout. However, he neglected the influence of quantum noise.

In this paper, we show that the above two approaches have to be combined and that noise plays an integral role in providing a quantitative understanding of the observed dropout phenomenon in the solitary laser near threshold with feedback. We show through a novel set of experiments, which involve modulating the pumping current or the feedback strength, that the Lang–Kobayashi model with feedback and spontaneous emission noise provides an excellent quantitative comparison with observations for three different cases. For all three cases, namely (1) no modulation of the pumping current or feedback strength, (2) sinusoidal modulation of the pumping current[12] only and (3) sinusoidal modulation of feedback strength only, the role of noise is critical in modeling to obtain excellent agreement with the observations. Also a simple explanation of the observed dropout phenomenon based on the adiabatic changes in the solutions on the ellipse in the parameter space spanned by the population inversion and the external cavity round trip phase shift, caused by the slow time modulation of the injection current or the feedback strength, is presented.

2. Experimental Setup and Observations

In the experiment (Fig. 1), a temperature controller is used to stabilize (to better then 0.01 K) a Fabry–Perot laser diode (Sharp LT015MD) with an anti-reflection coating of approximately 10% reflectivity on one facet and a high reflection coating on the other facet. The laser is pumped by a laser driver at the threshold current of 56.6 mA. A coupler (Picosecond, model 5547 bias-tee) coupling an AC signal on top of a DC signal is used between the laser driver and the diode. The light

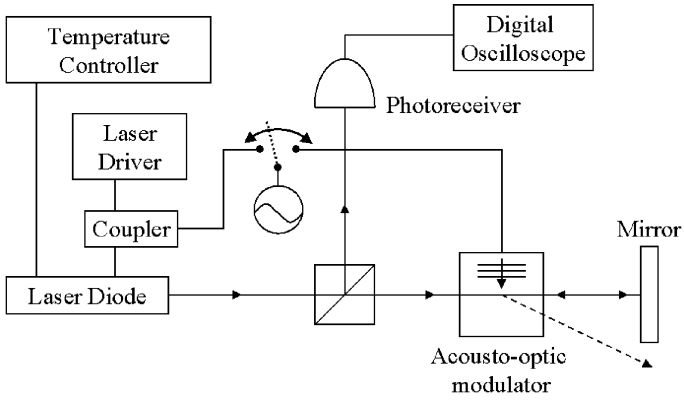

Fig. 1. Experimental setup.

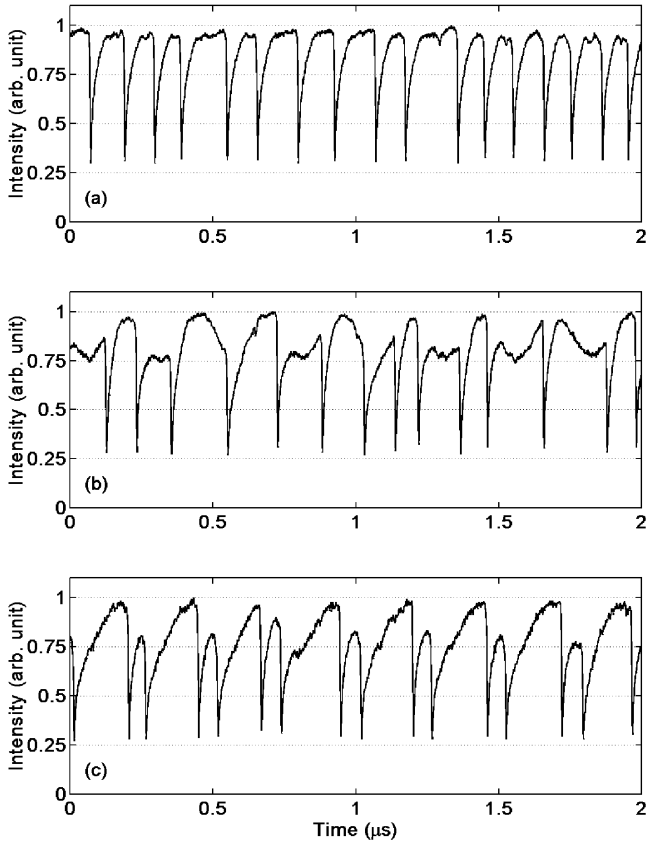

Fig. 2. Normalized intensity time series from experiment with sampling period of 800 ps with (a) no modulation, (b) current modulation, and (c) feedback modulation.

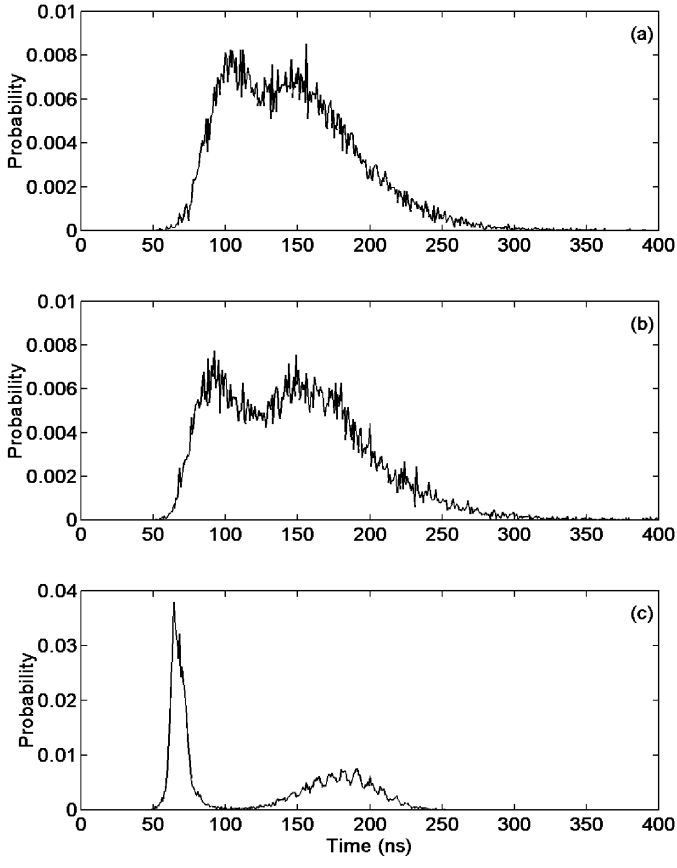

Fig. 3. Probability distribution function of the interval between two dropouts from experiment with (a) no modulation, (b) current modulation, and (c) feedback modulation.

(λ = 830 nm) from the diode is collimated by a microscope objective and then reflected by a mirror placed at a distance of 45 cm from the anti-reflection coated facet. An acousto-optic modulator (AOM) (ISOMET model 1206c) is inserted in the path of the reflected light to the laser. A beam splitter directs light onto a photoreceiver (New Focus Model 1181, DC-125MHz bandwidth). The output of the photoreceiver is recorded by a digital oscilloscope (Tektronix TDS7104). A 4 MHz sinusoidal signal, which is comparable in frequency to the inverse of the average dropout time interval without modulation, is fed to either the bias-tee to modulate the current or the AOM to modulate the feedback strength.

Shown in Figs. 2(a), 2(b), and 2(c) are the three cases. The first plot (a) shows the intensity dropout phenomenon as a function of time without any modulation of the pumping current or the feedback strength. The second one (b) is the same plot for which only the pumping current is modulated. The last case (c) is for feedback modulation only. The amplitude of the modulation is chosen such that the output

intensity fluctuation due to the modulation is about a quarter of the maximal output intensity of the laser with feedback. In Fig. 2(a), power dropout events occur irregularly due to the feedback. In Fig. 2(b), with current modulation, dropout events are superposed on top of a sine wave (associated with the modulation). Here the statistical behavior of the dropouts is not changed by the current modulation (Fig. 2(b)) compared to unmodulated case (Fig. 2(a)). This is clear through the random occurence of dropout events in both cases. However, for the case of feedback modulation (Fig. 2(c)), the dropout events are locked to the sine wave and occur only on the falling segment of the wave, which corresponds to a reduction of the feedback strength.

In Fig. 3, we show the probability distribution functions (PDFs) of the interval between consecutive dropouts for three cases. For the cases without modulation (Fig. 3(a)) and with current modulation (Fig. 3(b)), the PDFs show that both cases have similar dropout statistics. The two broad peaks observed in Figs. 3(a) and 3(b) are most probably due to mode-hopping of the laser between two solitary laser modes. Even in this case, current modulation appears to have a very small influence on the distribution. But the PDF for the feedback modulation case (Fig. 3(c)) indicates the frequency locking behavior by two clear peaks, the sharp one corresponding to the interval between two dropouts on one falling portion of the sine wave, while the broader peak corresponds to the longer interval between the dropouts on two consecutive falling phases of the sine wave. As a consequence, the statistical properties of the dropout events show a marked difference compared to the two previous cases. Thus current modulation and feedback modulation have dramatically different effects on the statistics of the dropout dynamics.

3. Numerical Model and Role of Noise

To understand these observations quantitatively, we integrated the Lang–Kobayashi equations given below[6]

$$\frac{dE}{dt} = \frac{1}{2}(1+i\alpha)G_{n,0}\sqrt{\frac{r_0}{r}}nE(t) + \kappa E(t-\tau)e^{-i\omega_0\tau} + F_E(t)\,, \tag{1}$$

$$\frac{dn}{dt} = (P-1)\frac{N_{th}}{\tau_r} - \Gamma_n|E|^2 - n\left(\frac{1}{\tau_r} + G_{n,0}\sqrt{\frac{r_0}{r}}|E|^2\right), \tag{2}$$

using a standard fourth order Runge–Kutta method. Here $E(t)$ is the complex field; $n(t) \equiv (N(t) - N_{th})$ is the difference between the carrier number at arbitrary time and the threshold carrier number $N_{th} = 3.9 \times 10^8$; $\alpha = 5$ is the linewidth enhancement factor; $G_{n,0} = 21400\ \mathrm{s}^{-1}$ and $r_0 = 0.32$ are the differential gain and facet power reflectivity of a laser with uncoated facet, respectively; $r = 0.1$ is the facet power reflectivity of a laser with an anti-reflection coating; $\kappa = (1 - r)(R/r)^{1/2}/\tau_{in}$ is the feedback rate, where $R = 0.05$ is the external mirror power reflectivity, $\tau_{in} = 3.9$ ps is the solitary laser pulse round trip time; $\tau = 3.0$ ns is the external cavity round trip time; ω_0 is the solitary laser frequency; $F_E(t)$ is

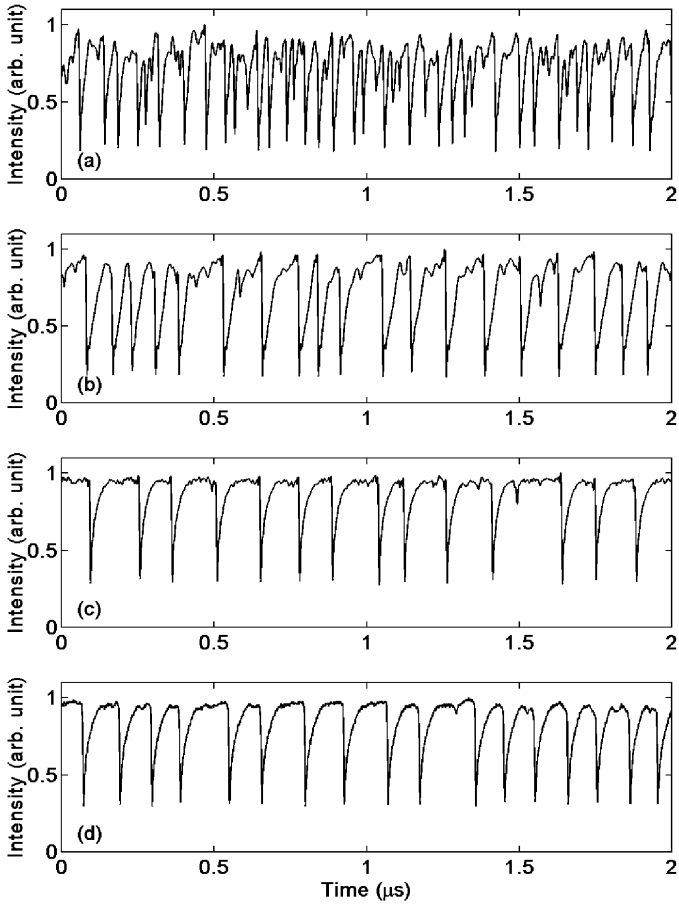

Fig. 4. Normalized intensity time series from simulation with (a) $R_{sp} = 0$ s^{-1}, (b) $R_{sp} = 10^{10}$ s^{-1}, (c) $R_{sp} = 10^{14}$ s^{-1} and (d) experiment with sampling period of 800 ps.

the Langevin noise term, with $\langle F_E(t)F_E(t')^* \rangle = R_{sp}\delta(t - t')$, where R_{sp} is the spontaneous emission rate; $P = 1.01$ is the ratio of pumping to threshold current; $\tau_r = 1.1$ ns is the carrier recombination time and $\Gamma_n = 1.1$ ps^{-1} is the photon decay rate. The constant value of $\omega_0\tau$ is taken to be a multiple of 2π for convenience. The equations are integrated with a time step of 0.5 ps from $t = 0$ to 3 μs and we display the last 2 μs only in order to remove the transient behavior influenced by initial conditions. The original time series are then Fourier transformed and a 125 MHz bandwidth low pass filter is applied to simulate the photoreceiver electronics.

In Fig. 4, we show the dropout intensity time series from simulations for three different spontaneous emnission rates, $R_{sp} = 0$ (Fig. 4(a)), 10^{10} (Fig. 4(b)) and 10^{14} s^{-1} (Fig. 4(c)) without modulation, respectively. We see that with the increment of the noise rate, the dropouts occur less and less frequently, and the shape of an individual dropout looks closer and closer to that in the experiment (Fig. 4(d)).

Finally, the simulation with $R_{sp} = 10^{14}$ s^{-1} (Fig. 4(c)) produces dropout phenomenon matching the experimental result (Fig. 4(d)) very well. It is worth mentioning that we tried combinations of different values for the parameters in the equations to simulate intensity time series which best match the experimental one without the spontaneous emission noise, namely, with a purely deterministic model, but we failed to do so. We conclude that we reproduce the experimental results only when we include a suitable amount of spontaneous noise ($R_{sp} = 10^{14}$ s^{-1}) in the model. This same level of noise will be used in all subsequent computations.

The importance of spontaneouse emission noise can further be investigated by introducing modulations on pumping current and feedback strength in the simulation. For the current modulation case, P is replaced by $P + A_I \sin(2\pi\nu_I t)$, where $A_I = 0.0045$ is current modulation amplitude, $\nu_I = 4 \times 10^6$ Hz is modulation frequency; if the feedback strength is modulated, R is replaced by

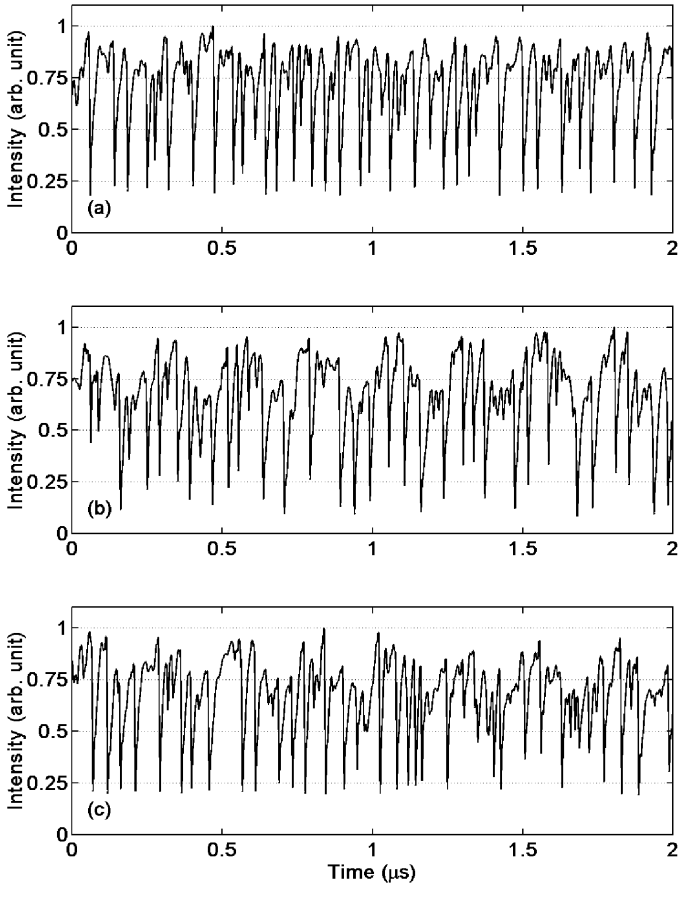

Fig. 5. Normalized intensity time series from simulation without noise with (a) no modulation, (b) current modulation, and (c) feedback modulation.

$R[(1 - A_R) + A_R \sin(2\pi\nu_R t)]$, where $A_R = 0.2$, $\nu_R = 4 \times 10^6$ Hz. Again, the amplitude of the modulation is chosen such that the output intensity fluctuation due to the modulation is about a quarter of the maximal output intensity of the laser with feedback.

Figures 5(a), 5(b), and 5(c) show the numerically computed intensity time series without modulation, with current modulation and with feedback modulation, respectively, ignoring $F_E(t)$. In Fig. 5(a), the dropout events occur much more frequently than those observed in the experiment (Fig. 2(a)). In Figs. 5(b) and 5(c), Neither the current nor the feedback modulation change the behavior of dropout events in the simulations, unlike the observations, where feedback modulation locks the dropouts (Fig. 2(c)). Also, the dropout events occur both on the raising and falling segments of the sine wave under feedback modulation in Fig. 5(c). Basically, without the Langevin noise term in the equations, the numerical modeling shows that all three cases have similar dropout characteristics, unlike the observations in Fig. 2.

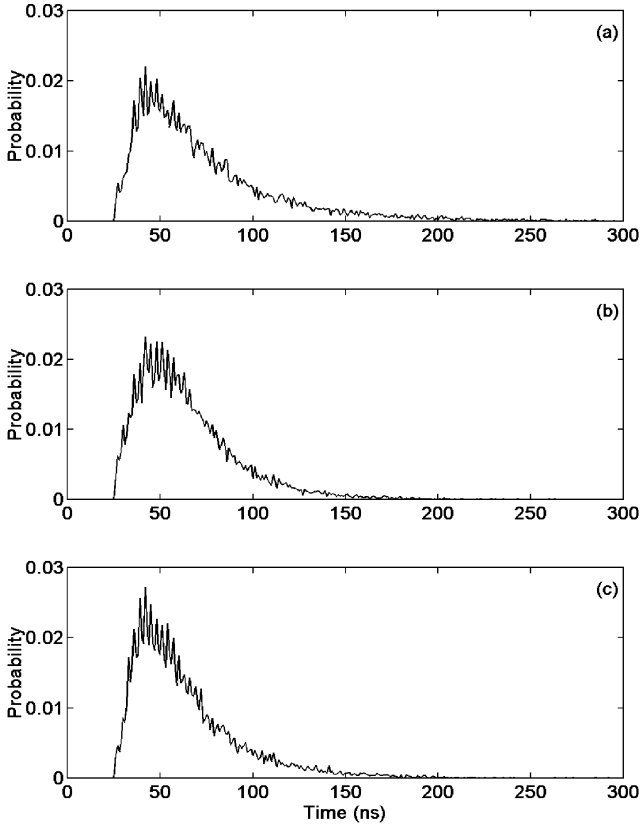

Fig. 6. Probability distribution function of the interval between two dropouts from simulation without noise with (a) no modulation, (b) current modulation, and (c) feedback modulation.

In Fig. 6, the PDFs of the interval between two dropouts from simulations without noise for three different cases confirm that the dropout statistics is not appreciably changed by either current or feedback modulations. All three cases have similar shape of PDF (Figs. 6(a), 6(b) and 6(c)).

In Fig. 7, the same three sets of simulations were repeated including the Langevin term $F_E(t)$. We can see that with the noise term, the experimental results in Fig. 2 are dramatically reproduced. In Fig. 7(a), the number of dropouts is significantly reduced compared to Fig. 5(a) and in 2 μs they occur at time scales comparable to those in the experiment (Fig. 2(a)). In Fig. 7(b), the current modulation doesn't change the statistics of the dropouts again in agreement with observations (Fig. 2(b)). Finally the most significant result is in Fig. 7(c), where the simulations show that feedback modulation in the presence of noise organizes the dropouts periodically on the falling edge of the sine wave, again in excellent agreement with the observations (Fig. 2(c)).

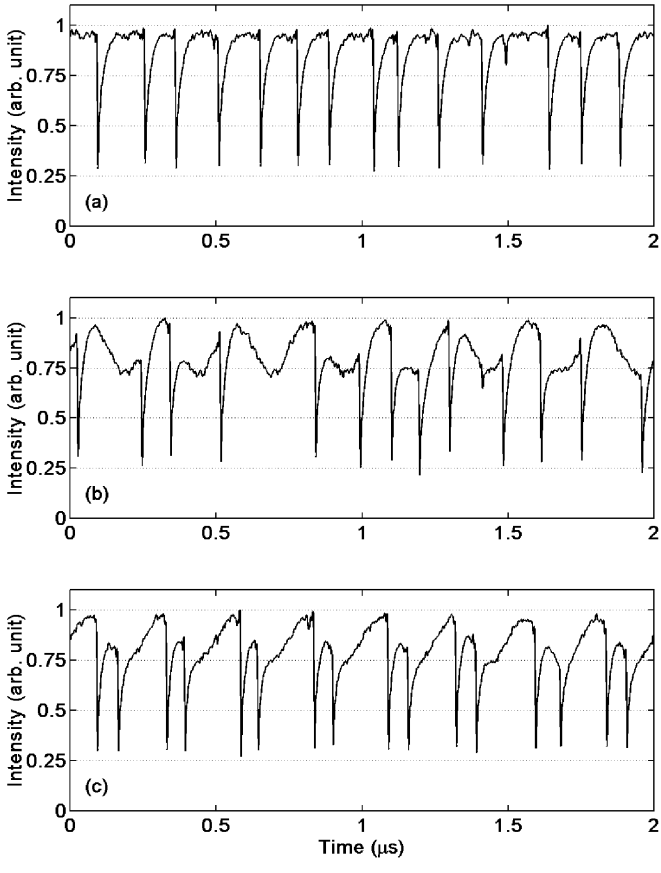

Fig. 7. Normalized intensity time series from simulation with noise with (a) no modulation, (b) current modulation, and (c) feedback modulation.

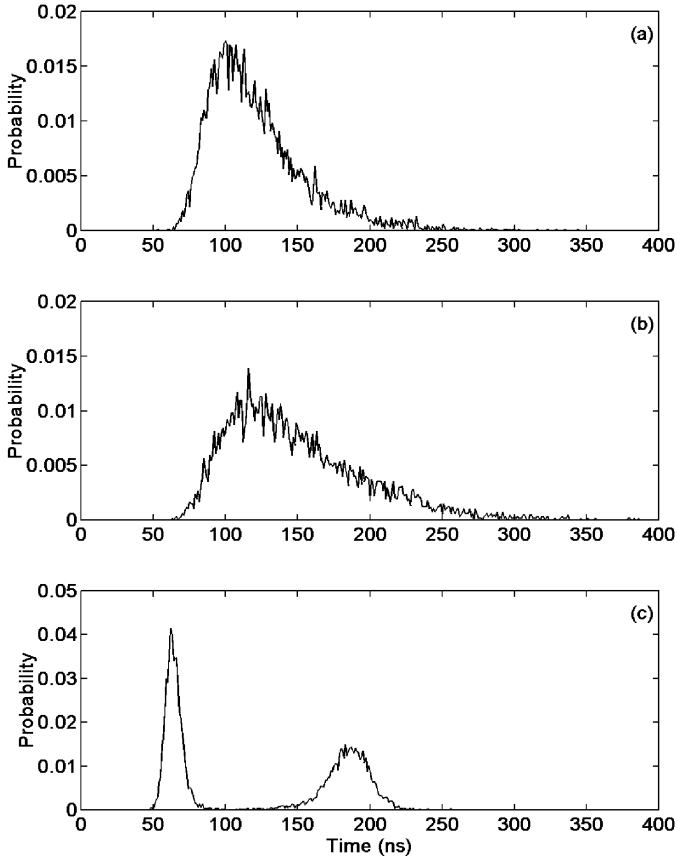

Fig. 8. Probability distribution function of the interval between two dropouts from simulation with noise with (a) no modulation, (b) current modulation, and (c) feedback modulation.

Figure 8 shows the PDFs of the interval between two dropouts from simulations with noise for three different cases. In Figs. 8(a) and 8(b), the two similar PDFs show that the cases without modulation and with current modulation from the simulation with noise have similar dropout statistics, whereas that of the feedback modulation case in Fig. 8(c) shows a two-peaked structure similar to Fig. 3(c), which indicates frequency locking behavior, as explained earlier.

4. Dynamics of Phase Space and the Effect of Modulation

In order to explain the phenomenon presented above, we follow Sano's approach[4] by examining the dynamics in the phase space spanned by population inversion $n(t)$ and the external cavity round trip phase shift $\phi(t) - \phi(t - \tau)$, where $\phi(t)$ is the phase of wave field $E(t)$. We first calculate the steady state solutions of the system by substituting $E(t) = \sqrt{P_s}e^{i\Delta\omega_s t}$, and $n(t) = n_s$ into Eqs. (1) and (2), setting $t = \tau$ in order to calculate one round trip phase shift $\Delta\omega_s\tau$ and obtaining

the following three transcendental equations:[5]

$$\Delta\omega_s\tau = -\kappa\tau\sqrt{1+\alpha^2}\sin(\omega_0\tau + \tan^{-1}\alpha + \Delta\omega_s\tau)\,, \tag{3}$$

$$n_s = -2\kappa G_{n,0}\sqrt{r/r_0}\cos(\omega_0\tau + \Delta\omega_s\tau)\,, \tag{4}$$

$$P_s = \frac{(P-1)N_{th} - n_s}{\tau_r(\Gamma_n + n_s G_{n,0}\sqrt{r_0/r})}\,. \tag{5}$$

We solve for $\Delta\omega_s\tau$ in Eq. (3) by Newton's method and obtain 1589 solutions, which can then be substituted into Eq. (4) to get the corresponding n_s, and into Eq. (5) to get P_s. From Eqs. (3) and (4), we know that the set of steady state solutions $(\Delta\omega_s\tau, n_s)$ form an ellipse in the phase space of $n(t)$ and $\phi(t) - \phi(t-\tau)$. According to Sano's definition, the solutions forming the upper brench of the ellipse are called "antimodes", while those forming the lower branch are external cavity modes. For our choice of parameters, the "steady" state external cavity mode solutions are unstable and chaotic in the absence of noise. This is the intrinsic deterministic chaos in the feedback laser system. The chaotic attractors are located in the vicinity of the unstable steady states. This is why the basic steady state solutions, even if they are unstable, provide a reliable framework for understanding the dynamics. In Fig. 9(a), the trajectory of simulation without noise and modulation is plotted on top of the ellipse. During the recovery part of the dropout, the trajectory "tunnels" from one steady state to the next with large deviations on the chaotic attractors. The dropout occurs when the chaotic attractors associated with the unstable steady states on the lower section of the ellipse, collide with the unstable "antimodes" on the upper section of the ellipse, and the trajectory relaxes towards zero inversion and phase shift, which is the steady state of the solitary laser without feedback. Because of the feedback, the trajectory starts from the upper right of the lower branch of the ellipse and the intensity recovers again. The dynamics on the chaotic attractors progresses towards the highest external cavity gain mode. This is intercepted by a random collision with the "antimodes" again, and the process repeats itself.

If the noise is included in the simulation, then it introduces coherence by allowing the "tunneling" from one steady state to the next without very large deviations on the chaotic attractor. This is clearly shown in Figs. 9(b) and 9(c), where two different values of noise rate $R_{sp} = 10^{10}$ and 10^{14} s^{-1} are used respectively. We see that with the increment of noise rate, the fluctuation of the trajectory on the attractors in $n(t)$ coordinate becomes smaller and smaller, so it takes a longer and longer time to go through more external cavity modes and then collide with an "antimode". The dropouts therefore occur less and less frequently (Fig. 4(a) to 4(c)). Here we see how the noise affects the dynamics of the system in an counter-intuitive way — *it reduces the fluctuations and organizes the dynamics of the system.*

With the *same* spontaneous emission noise level 10^{14} s^{-1}, now let us discuss the two cases in which we modulate either the pumping current or the feedback strength. We recall that the modulation frequency used in these investigations is very small (about two order of magnitude) compared to the frequency

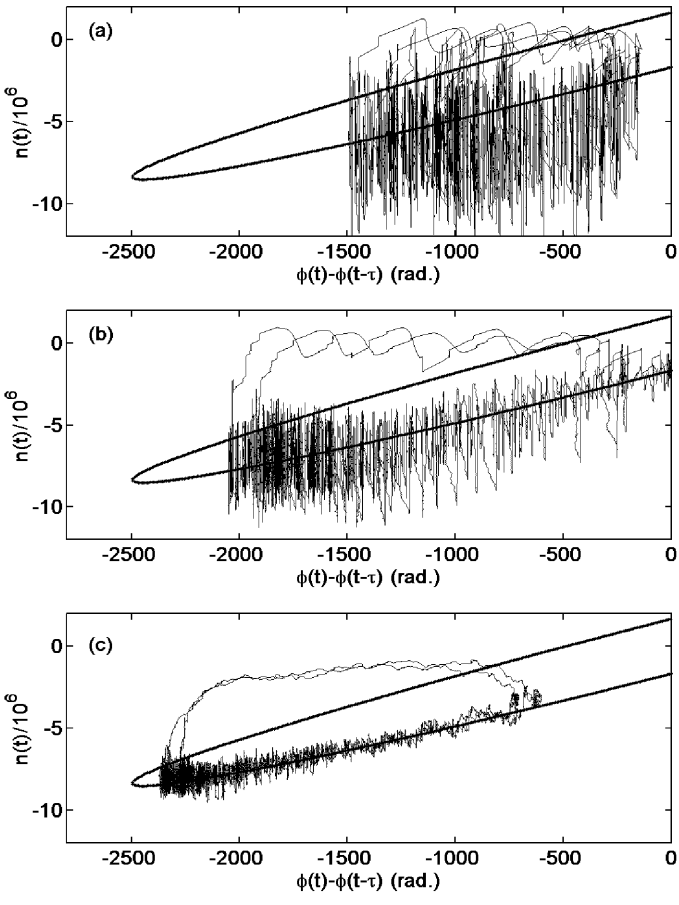

Fig. 9. Phase space of population inversion and phase shift for (a) $R_{sp} = 0$ s^{-1}, (b) $R_{sp} = 10^{10}$ s^{-1}, (c) $R_{sp} = 10^{14}$ s^{-1}.

difference between the external cavity modes. As a consequence, these modulations *adiabiatically* move the steady state solutions in the phase space of $\phi(t) - \phi(t-\tau)$ and n_s or P_s. Now, if we slowly modulate the pumping current, P becomes a time dependent quantity. Since there is no dependence on P in Eqs. (3) and (4), the steady state solutions, $\Delta\omega_s\tau$ and n_s, and therefore the ellipse, are fixed. So the attractors in the phase space of $n(t)$ and $\phi(t) - \phi(t-\tau)$ collide with the "antimodes" on the upper branch of the ellipse at about the same position (Fig. 10(b)) as the case without modulation (Fig. 10(a)) for each dropout. Therefore, the dropout statistics is the same without modulation and with current modulation.

On the other hand, for the case of feedback modulation, both $\Delta\omega_s\tau$ and n_s change according to Eqs. (3) and (4). In fact, the number of steady solutions oscillates between 1231 and 1589. Again, since the modulation frequency is very small compared to the external cavity modes frequencies, this leads to an adiabatic

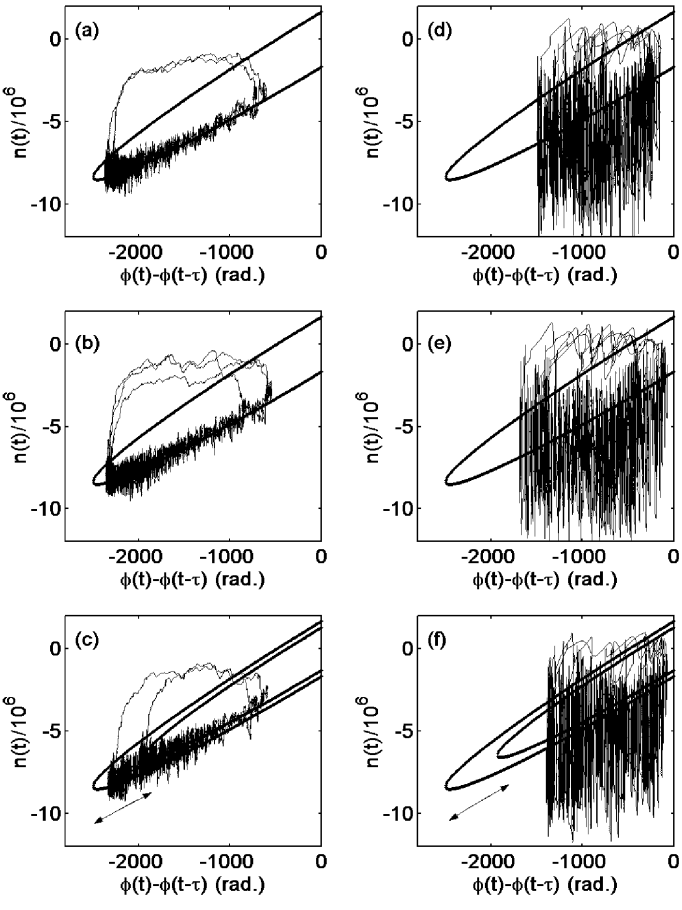

Fig. 10. Phase space of population inversion and phase shift for (a)–(c) simulation with noise, and (d)–(f) simulation without noise. (a) and (d) no modulation, (b) and (e) current modulation and (c) and (f) feedback modulation.

motion of the steady state solutions in the population inversion and phase shift space. In Fig. 10(c), the two ellipses with the most and least number of solutions corresponding to maximal and minimal feedback strength respectively are plotted. Feedback modulation moves the ellipse between these two extremes. When the feedback strength is increasing (decreasing), represented by the increasing (falling) segment of the sine wave on the intensity time series (Fig. 7(c)), the ellipse moves toward lower left (upper right), in the same (opposite) direction as the trajectory in phase space (Fig. 10(c)). So the collision between the attractors on the lower branch of the ellipse and the "antimodes" is inhibited (enhanced). Therefore the dropout can not (can) occur. This is precisely why in Figs. 2(c) and 7(c), the dropouts are observed to occur during the falling phase but not in the rising phase of the modulational cycle.

Also shown in Fig. 10(d) to Fig. 10(f), are the three corresponding plots for simulations *without* noise. In Fig. 10(d), the fluctuation on the chaotic attractor is much larger in the $n(t)$ direction compared to the case with noise (Fig. 10(a)). Only a small section on the lower branch of the ellipse is traversed before a collision between the attractors and the upper unstable branch of the ellipse occurs. So the collisions, and therefore the dropouts, occur here more frequently (Fig. 5(a)) than in the system with noise (Fig. 7(a)). In Fig. 10(e), current modulation doesn't change the ellipse and the trajectory on the fixed ellipse looks similar to that in Fig. 10(d). In Fig. 10(f), under the absence of noise, the fluctuation of the dynamics is so large that the chaotic attractors collide with the "antimodes" frequently and the collisions are not influenced by the slow oscillation of the ellipse due to feedback strength modulation. Thus collisions with the upper branch can occur for both the motions of the ellipse, towards and opposite to the direction of the trajectory. Consequently, the dropouts can occur on both phases of the sinusiodal modulation (Fig. 5(c)).

The ellipse dynamics caused by the modulations with consequence on dropouts can also be seen in the alternate phase space of intensity and phase shift $\phi(t) - \phi(t-\tau)$. Now the steady states form a "distorted" ellipse (Fig. 11). In Fig. 11(a), the phase dynamics corresponding to two consecutive dropouts is plotted on top of the distorted ellipse. During the recovery part of the dropout, the trajectory climbs along the upper branch of the distorted ellipse. When it is close to tip of the ellipse (maximal gain output), the dropout occurs, represented by the fast drop of the intensity followed by relaxation of the phase shift to zero. The power dropout phenomenon in time domain is therefore represented by a continuous winding curve in this phase space.

For the current modulation case, P is time dependent. From Eqs. (3) and (5), we see that although the solutions of phase shift $\Delta\omega_s\tau$ are fixed, the solutions, P_s, change with time. Therefore the distorted ellipse only changes the position, but not the size in the phase space. In Fig. 11(b), the upper and lower distorted ellipses correspond to the set of steady state solutions for the maximal and minimal pumping current. The current modulation adiabatically moves the ellipse vertically between these two extremes. The trajectory of intensity $P(t)$ versus phase shift $\phi(t) - \phi(t-\tau)$ is again a continuous winding curve, corresponding to time series in Fig. 7(b). The trajectory follows the moving reference frame (the distorted ellipse), caused by the modulation, and the positions of dropouts on the frame are not affected by the motion of the frame. Therefore current modulation has the same dropout statistics as the unmodulated case (Fig. 7(a)), except for the sinusoidal modulation of the peak intensity (Fig. 7(b)).

For feedback modulation, both P_s and $\Delta\omega_s\tau$ and therefore both the size and the position of the distorted ellipse change with time. In Fig. 11(c), the upper left and lower right distorted ellipses correspond to the maximal and minimal feedback strength. The sinusoidal modulation moves the ellipse between these two extremes. The dropouts are inhibited (enhanced) when the feedback strength is increasing

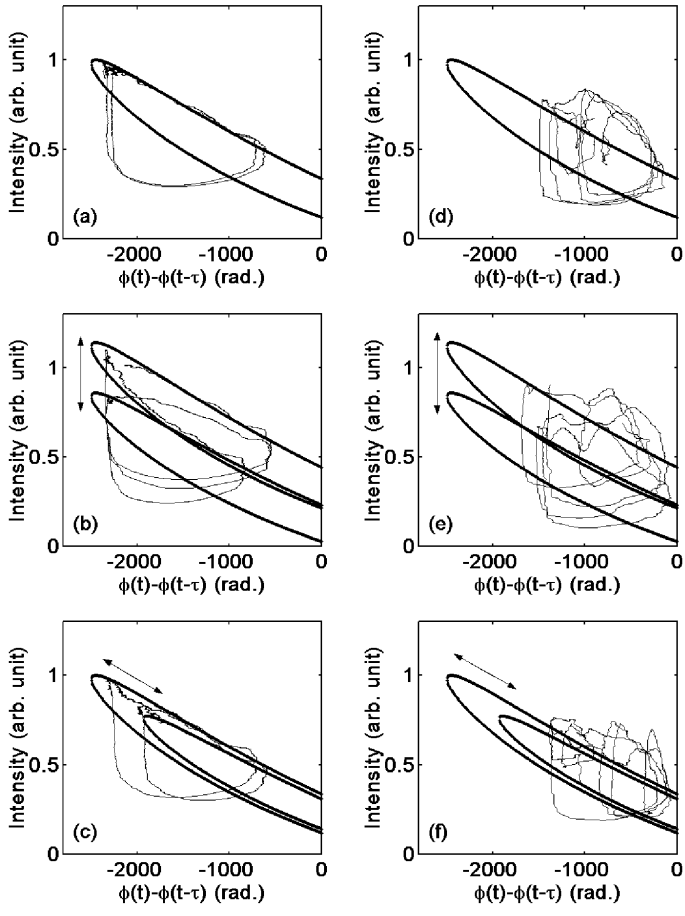

Fig. 11. Phase space of intensity and phase shift for (a)–(c) simulation with noise, and (d)–(f) simulation without noise. (a) and (d) no modulation, (b) and (e) current modulation and (c) and (f) feedback modulation.

(decreasing), which correspond to the upper left (lower right) movement of the ellipse. As a result, the dropouts occur periodically on the falling phase of the sinusoidal feedback modulation (Fig. 7(c)).

In Fig. 11(d) to Fig. 11(f), the three corresponding plots for simulations without noise show that different kinds of modulations (or no modulation) do not follow the moving frame. And all three cases have much more frequent dropout events (Fig. 5(a) to 5(c)). However, in the case of the current modulation, the maximal intensity does show the modulation (Fig. 5(b) and Fig. 11(b)).

5. Conclusions

The role of noise on the dropout phenomenon observed in semiconductor lasers near threshold with optical feedback, is highlighted by modulating the pumping current

and the feedback strength. In the experiment, the two cases produce totally different dropout dynamics. In the former, the dropouts occur randomly; in the later, they are locked by the sinusoidal modulation periodically on the falling edge of the wave.

In the simulation, different levels of spontaneous emission rate show that the noise reduces the fluctuation of the dynamics in the phase space and the frequency of the power dropouts. An optimal value is therefore found to match the experimental and numerical results well. This same level of noise is used in the following calculation.

With current modulation, the motion of the distorted ellipse due to the modulation and the trajectory in phase space of intensity and phase shift are orthogonal to each other and hence no coupling occurs between them. Therefore, the current modulation does not change the dropout dynamics. However with feedback modulation, the motions of the ellipse and the trajectory are in parallel and both dynamics couple with each other in both phase spaces. This leads to the occurence of the dropouts only during the falling phase of the modulation.

By modeling the observed features using the Lang–Kobayashi equations with a Langevin noise source, we have identified that only in the presence of noise (which was taken to be the same for all three cases) can the distinct behaviors for the two different types of modulation be explained. Simulations without noise show that the large fluctuations on the chaotic attractor dominate the dynamics thereby obscuring and significantly reducing the role of modulation in the injection current and the feedback constant.

Acknowledgments

We gratefully acknowledge support from the Office of Naval Research (Physics) and extensive discussion with Dr. David W. Sukow.

References

1. R. Lang and K. Kobayashi, *IEEE J. Quantum Electron.* **QE-16**, 347 (1980).
2. C. H. Henry and R. Kazarinov, *IEEE J. Quantum Electron.* **QE-22**, 294 (1986).
3. J. Mørk, J. Mark and B. Tromborg, *Phys. Rev. Lett.* **65**, 1999 (1990).
4. T. Sano, *Phys. Rev.* **A50**, 2719 (1994).
5. G. H. M. van Tartwijk, A. M. Levine and D. Lenstra, *IEEE J. Select. Topic Quantum Electron.* **1**, 466 (1995).
6. A. Hohl, H. J. C. van der Linden and Rajarshi Roy, *Opt. Lett.* **20**, 2396 (1995).
7. I. Fischer *et al.*, *Phys. Rev. Lett.* **76**, 220 (1996).
8. M. Giudici *et al.*, *Phys. Rev.* **E55**, 6414 (1997).
9. G. Vaschenko *et al.*, *Phys. Rev. Lett.* **81**, 5536 (1998).
10. A. Hohl and A. Gavrielides, *Phys. Rev. Lett.* **82**, 1148 (1999).
11. D. Sukow *et al.*, *Phys. Rev.* **60**, 667 (1999).
12. D. Sukow *et al.*, *IEEE J. Quantum Electron.* **QE-36**, 175 (2000).
13. C. Masoller, *Phys. Rev. Lett.* **88**, 34102 (2002).